Collisional excitation of C2H- by H2: New interaction potential and scattering calculations

Fabien Dumouchel, Ernesto Quintas-Sánchez, Christian Balança, Richard Dawes, François Lique, Nicole Feautrier

APS
Submitted to J. Chem. Phys.

Collisional excitation of C_2H^- by H_2: new interaction potential and scattering calculations

Fabien Dumouchel,[1, a)] Ernesto Quintas-Sánchez,[2] Christian Balança,[3] Richard Dawes,[2] François Lique,[4] and Nicole Feautrier[3]

[1)] *LOMC - UMR 6294, CNRS-Université du Havre, 25 rue Philippe Lebon, BP 1123, 76 063 Le Havre cedex, France*

[2)] *Department of Chemistry, Missouri University of Science and Technology, Rolla, MO 65409, USA*

[3)] *Observatoire de Paris, Université PSL, CNRS-UMR 8112, LERMA, F-92195 Meudon, France*

[4)] *Univ. Rennes, CNRS, IPR (Institut de Physique de Rennes) - UMR 6251, F-35000 Rennes, France*

(Dated: 10 April 2023)

Interstellar anions play an important role in astrochemistry as being tracers of the physical and chemical conditions in cold molecular clouds and circumstellar gas. The local thermodynamic equilibrium (LTE) is generally not fulfilled in media where anions are detected and radiative as well collisional data are required to model the observed lines. The C_2H^- anion has not yet been detected in the interstellar medium; however, collisional data could be used for non-LTE models that would help in identifying the most intense lines. For this purpose, we have computed the first 4D potential energy surface (PES) of the C_2H^-–H_2 complex using an explicitly correlated coupled-cluster approach. The PES is characterized by a single deep minimum with a well-depth of 924.96 cm^{-1}. From this interaction potential, we derived excitation cross sections and rate coefficients of C_2H^- induced by collisions with *para*- and *ortho*-H_2. The results obtained for collisions with *para*-H_2 are compared to previous calculations performed using a 2D-PES obtained from an average over H_2 rotations.

[a)] Electronic mail: fabien.dumouchel@univ-lehavre.fr

I. INTRODUCTION

Although the presence of anions in astrophysical environments was predicted theoretically and introduced into chemical models in the 80's,[1,2] the first negative anion, C_6H^-, was detected only in 2006,[3] solving a problem of unidentified lines discovered by Kawaguchi *et al.*[4] This was followed by the detection of other anions, such as C_4H^-,[5–7] C_8H^-,[8–10] CN^-,[11] C_3N^-,[12] C_5N^-,[13] and very recently C_7N^-.[14] The majority of these species were first detected and observed in the circumstellar envelope of IRC+10216, and later in cold molecular clouds.[7]

The discovery of carbon chain anions in interstellar and circumstellar environments has stimulated a lot of theoretical and experimental work. Indeed, their role in interstellar chemistry has been the object of many studies.[15–19] However, the formation of negative ions in space is still not well understood.

In 1980, Sarre discussed[15] the formation and the possible detection of C_2H^- in the interstellar medium (ISM) but did not calculate its abundance. Although C_2H^- has been observed in the laboratory,[10,20] and its neutral form C_2H is a well-known interstellar molecule discovered in 1974,[21] the C_2H^- anion seems to be a very low-abundant species and has not been detected until now, with only a low upper limit in IRC+10216 being given.[6] Despite that the formation of many of the hydrocarbon anions is not yet solved, the very low abundance of C_2H^- seems to be justified by the very high chemical reactivity of this anion leading to its destruction very quickly after its formation. In fact, in addition of its highest reactivity, current numerical models predict that this anion is not efficiently formed through the $C_2H + e^-$ association, while, even if debated, the formation rates increase with increasing size of the carbon chain.[22,23]

In the laboratory, cooling and controlling molecular ions in cold traps is an important topic as anions are, through photodetachment, precursors of cold molecules with many applications.[24,25] Collisions with a He buffer gas in the trap play a major role for the preparation of the ions in specific vibrational and rotational states. However, in a recent study, Mant *et al.*[26] consider possible cooling by H_2 instead of He as collisional cross sections by H_2 are much larger than cross sections with noble gas atoms, leading to faster thermalization times.[27]

The C_2H^-–H_2 collisional data are then needed in cold physics studies and they can also

help in searching for C_2H^- by informing non-Local Thermodynamic Equilibrium (LTE) models, which would predict the most intense lines. Recently, rate coefficients for collisions with *para*-H_2 were obtained using a reduced 2D-Potential Energy Surface (PES) averaged over three H_2 orientations.[28] However, because of the strong anisotropy of the interaction PES with respect to the orientation of H_2 usually found for ionic species, the use of a reduced dimension PES could lead to inaccuracies in the determination of *para*-H_2 rate coefficients, as found recently for NS^+–H_2 collisions.[29] Moreover, calculations with a 2D-PES do not allow to obtain the data for collisions with *ortho*-H_2, much needed for the non-LTE modeling of media where both *para*- and *ortho*-H_2 are considered important colliders.

In this paper, we report the first 4D C_2H^-–H_2 interaction PES and inelastic cross sections and rate coefficients for C_2H^- induced by both *para*- and *ortho*-H_2. The *ab initio* PES was computed using an explicitly-correlated coupled-cluster *ab initio* approach. Quantum scattering calculations were performed to compute collisional cross sections and rate coefficients between the lowest 11 rotational levels of C_2H^-. Details of the electronic structure calculations are given in Section 2 while Section 3 provides a brief description of the scattering calculations. The results are shown and discussed in Section 4 and concluding remarks are given in Section 5.

II. POTENTIAL ENERGY SURFACE

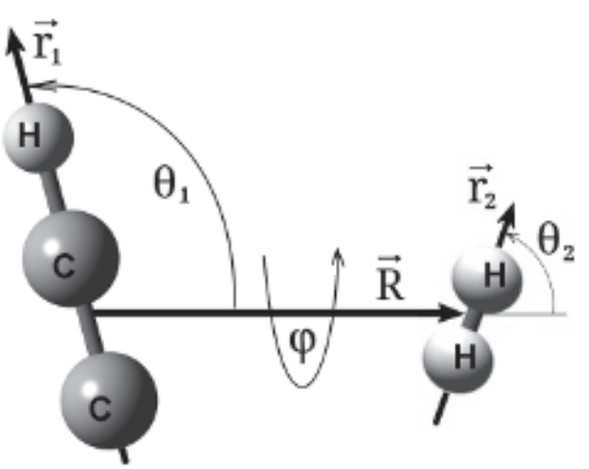

FIG. 1. Coordinates used to describe the C_2H^-–H_2 interaction. See the text for details.

In the ground electronic state, C_2H^- is a linear singlet ($X^1\Sigma^+$). As depicted in Fig. 1,

the coordinates used to describe the four-dimensional (4D) C_2H^-–H_2 PES are the Jacobi coordinates R, θ_1, θ_2, and φ. $\vec{R}$ is the vector between the centers of mass of the two fragments, and $\vec{r}_1$ and $\vec{r}_2$ are vectors aligned with each molecule. Coordinate R is the length of vector $\vec{R}$, while coordinates θ_1 and θ_2 represent (respectively) the angles between $\vec{R}$ and the vectors $\vec{r}_1$ and $\vec{r}_2$. The fourth coordinate is the dihedral (out of plane) torsional angle, labeled φ, which is the angle between the vectors $\vec{R}\times\vec{r}_1$ and $\vec{R}\times\vec{r}_2$. Notice that for $\theta_1 = 0°$ the C_2H^- molecule aligns with the H atom pointing to the center-of-mass of the H_2 molecule.

A. Electronic structure calculations

For the construction of the PES, both monomers were held rigid. The bond distance for H_2 was fixed at $r_{HH} = 0.76665$ Å, the vibrationally-averaged bond distance for the ground rovibrational state of H_2. For C_2H^-, the equilibrium geometry is linear, and the distances employed in this study ($r_{CC} = 1.25164$ Å and $r_{CH} = 1.05963$ Å) were obtained by geometry optimization at the (AE)CCSD(T)-F12b/CVQZ-F12 level where (AE) indicates that all electrons were included in the correlation treatment. The final high-level PES was computed using explicitly-correlated coupled-cluster theory[30] (CCSD(T)-F12b). The complete basis set limit was estimated by extrapolating calculations at the (AE)CCSD(T)-F12b/CVTZ-F12 and (AE)CCSD(T)-F12b/CVQZ-F12 levels[31] using the l^{-3} formula.[32] A *geminal beta* coefficient value of 1.5 was specified for the F12 calculations which include the correlation of core electrons. As mentioned below, to avoid placing expensive high-level data in energetically inaccessible regions, a lower-level guide surface was first constructed. This was done using data at the CCSD(T)-F12b/VDZ-F12 level of theory. Exploiting the system's symmetry, energies were only computed in the reduced angular range: $0 < \theta_1 < 180°$, $0 < \theta_2 < 90°$, and $0 < \varphi < 180°$. All *ab initio* calculations were performed using the Molpro electronic structure code package.[33]

B. Analytical representation and characterization of the PES

As we have done in the past for other van der Waals (vdW) linear dimers,[34–41] the PES's analytical representation was constructed using an automated interpolating moving least squares (IMLS) methodology, freely available as a software package under the name

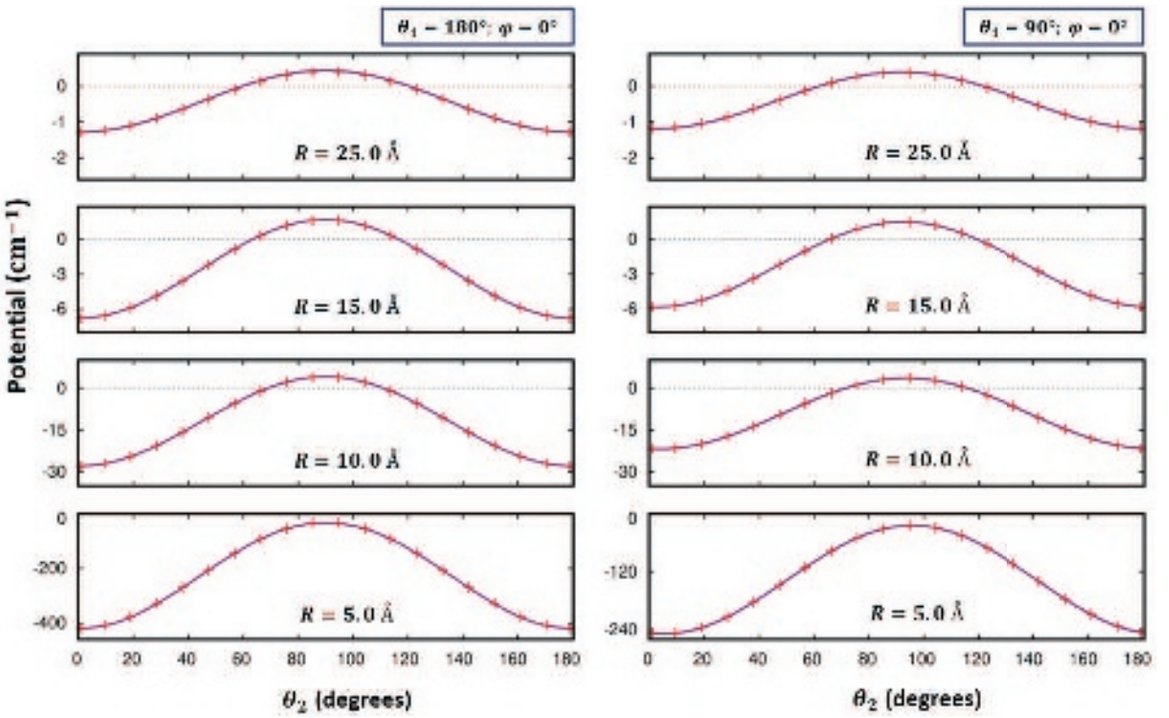

FIG. 2. 1D cuts of the C_2H^-–H_2 interaction energy as a function of angle θ_2 for four different intermolecular separations: R = 25.0, 15.0, 10.0, and 5.0 Å. The angles θ_1 and φ are fixed (at left) at 180° and 0°, and (at right) at 90° and 0° respectively. Lines represent the fitted PES, and crosses represent *ab initio* data (not used in the fit).

AUTOSURF.[42] As usual,[43,44] a local fit was expanded about each data point, and the final potential is obtained as the normalized weighted sum of the local fits. This interpolative approach can accommodate arbitrary energy-surface topographies, being particularly advantageous in systems with large anisotropy. The fitting basis and most other aspects of the IMLS procedure were the same as for other previous systems and have been described in detail elsewhere.[42,44,45]

The shortest intermonomer center-of-mass distance considered is R = 1.6 Å, with the additional restriction of a maximum repulsive energy of 6 kcal/mol ($\sim$ 2 100 cm^{-1}) above the separated monomers' asymptote. The *ab initio* data coverage in the fitted PES extends to R = 20 Å, which is extended by an analytic form, with the zero of energy set at infinite separation between the monomers. Additional data extending as far as R = 60 Å was used to determine and confirm the correct behavior of the long range form. As shown in Fig. 2, there is still a strong sensitivity to the orientation of the H_2 in the long range of the

PES, due to its leading electrostatic moment (quadrupole) interacting with the charge of the C_2H^- molecule. Indeed, *cf.* Fig. 2, the interaction energy still varies by more than 1.5 cm^{-1} with respect to θ_2 at $R = 25$ Å. A similar behavior has been previously observed when studying the CF^+–H_2 and HCS^+–H_2 vdW ion-molecule complexes.[35,41] In this system the dependence on the orientation of C_2H^- was also found to be significant, and so the analytic form of the long-range was constructed including both the charge-quadrupole and dipole-quadrupole (two leading) terms, which vary as R^{-3} and R^{-4} respectively. The impact of the dipole-quadrupole term and its R^{-4} dependence can be appreciated by comparing each pair of panels in Fig. 2. At $R = 25$ Å the two most attractive poses of $\theta_2 = 0$ or 180° (at the edges of the plots) are similar for $\theta_1 = 180°$ and 90° (left and right panels). However, following the same comparison at $R = 15$, 10 and 5 Å the $\theta_1 = 90°$ orientation plotted in the panels at right, becomes rapidly increasingly less attractive, highlighting the growing importance of the dipole-quadrupole term. The two-term form is sufficient to match the *ab initio* data well. Thus the global fit switches smoothly from interpolated *ab initio* data in the close interaction region to the analytic long range via a hyperbolic tangent function centered at $R = 15$ Å.

For the high-level PES, the global estimated root-mean-squared fitting error tolerance was set to 0.50 cm^{-1}, and the total number of automatically generated symmetry-unique points needed to reach that target was 2 400 (the final estimated error is 0.13 cm^{-1} for energies below the asymptote). To guide the placement of high-level data, as previously mentioned, a lower-level guide surface was constructed using 2 614 symmetry-unique points, distributed using a Sobol sequence[46] biased to sample the short-range region more densely. The analytical representation of the PES is available as supplementary material.

Figure 3 shows a 2D representation of the PES (denoted R-optimized) as a function of the angles θ_1 and θ_2 for planar configurations ($\varphi = 0°$). The plot describes the complete ranges of θ_1 and θ_2, relaxing the intermonomer distance coordinate R for each pair of angles. The PES is characterized by a single minimum (the two molecules aligned, with the H_2 at the C-end of the C_2H^-) with a well-depth of 924.96 cm^{-1}. The center-of-mass distance at the minimum is quite short for a collinear complex, at $R = 3.686$ Å (*cf.* Fig. 4).

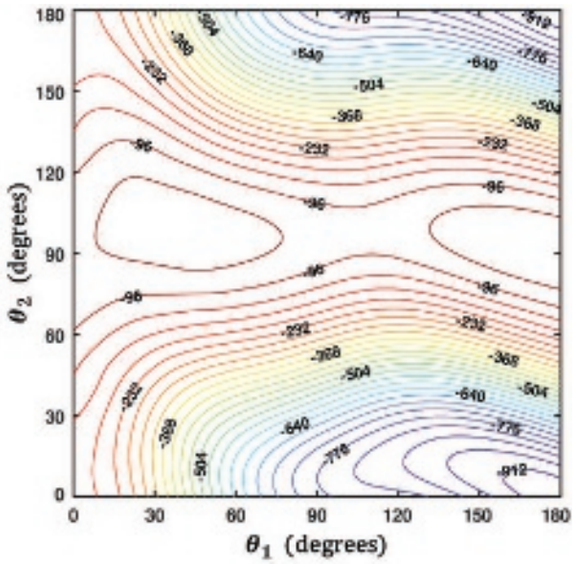

FIG. 3. R-optimized contour plot of the PES as a function of the angles θ_1 and θ_2 for planar configurations ($\varphi = 0°$). For each pair of angles, the energy (given in cm^{-1}) is optimized with respect to the center-of-mass distance R.

III. SCATTERING CALCULATIONS

The MOLSCAT nonreactive scattering code[47] was used to carry out scattering calculations of the rotationally inelastic cross sections for collisions between C_2H^- and both *para*- and *ortho*-H_2. The cross sections were computed using the quantum close coupling approach and the modified log-derivative Airy propagator[48] starting from $R_{min} = 4.8$ a_0 (2.54 Å) to $R_{mid} = 40$ a_0 (21.16 Å) for the log-derivative integration method and from R_{mid} to $R_{max} = 100$ a_0 (52.8 Å) for the Airy propagator integration. In the following, the rotational states of the C_2H^- and H_2 molecules are denoted j_1 and j_2 respectively, other molecule-related parameters are labeled 1 for C_2H^- and 2 for H_2.

The expansion of the potential $V(R, \theta_1, \theta_2, \varphi)$ over a suitable basis of angular functions for any intermolecular distance R was performed according to Green (1975)[49]

$$V(R, \theta_1, \theta_2, \varphi) = \sum_{l_1 l_2 l} v_{l_1 l_2 l}(R) A_{l_1 l_2 l}(\theta_1, \theta_2, \varphi), \tag{1}$$

where functions $A_{l_1 l_2 l}(\theta_1, \theta_2, \varphi)$ are contracted normalised spherical harmonics, $v_{l_1 l_2 l}(R)$ are the radial coefficients. In this work, the potential was expanded including $0 \leq l_1 \leq 15$ for the C_2H^- molecule and $0 \leq l_2 \leq 4$ for the H_2 molecule.

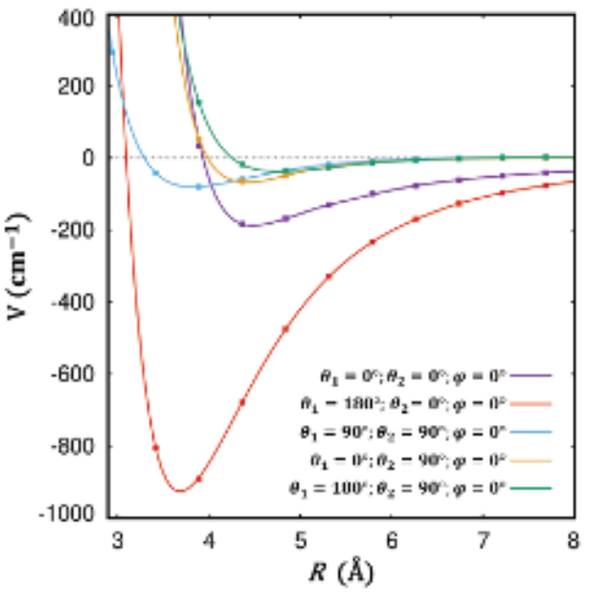

FIG. 4. Various radial cuts defined by different orientational poses of the monomers. In all cases, energies are in cm^{-1}, lines represent the fitted PES, and points represent *ab initio* calculations (not used in the fit).

For C_2H^-, we used the molecular constants of Brünken *et al.*,[10] $B_e = 1.3889354$ cm^{-1} and $D_e = 3.2345 \times 10^{-6}$ cm^{-1}. The molecular constants of H_2 were set to $B_e = 60.853$ cm^{-1}, $\alpha_e = 3.062$ cm^{-1}, and $D_e = 0.0471$ cm^{-1}. Inelastic cross sections were obtained between the first 11 rotational levels of C_2H^- ($0 \leq j_1 \leq 10$). The parameters of integration were chosen to ensure convergence of these cross sections for collisional kinetic energies ranging from 0.1 cm^{-1} up to 1000 cm^{-1}. At each energy, the maximum value of the total angular momentum J_{tot} needed to obtain cross sections converged to better than 5.0×10^{-3} $Å^2$ was automatically set by the MOLSCAT program. The size of the rotational basis was studied carefully in order to ensure convergence of the cross sections and to optimize the calculation in terms of CPU time.

The first 16 rotational levels of C_2H^- ($0 \leq j_1 \leq 15$) were included in the basis set as the cross sections resulting from larger basis sets (20 and 25 levels) differ by less than a few percent from the 15-levels choice (see Table I). Concerning the H_2 basis, two sets of calculations were performed for collisions with *para*- and *ortho*-H_2: calculations were done either with only the ground rotational state of *para*-H_2 and *ortho*-H_2 ($j_2 = 0$ and $j_2 = 1$

TABLE I. Cross sections at a collision energy of $E_c = 200$ cm^{-1} as a function of the size (j_{1max}) of the C_2H^- rotational basis. The rotational basis of *para*-H_2 and *ortho*-H_2 includes $j_2 = 0, 2$ and $j_2 = 1$, respectively.

		para-H_2			*ortho*-H_2		
j_1	j_1'	$j_{1max} = 15$	$j_{1max} = 20$	$j_{1max} = 25$	$j_{1max} = 15$	$j_{1max} = 20$	$j_{1max} = 25$
1	0	12.6	12.5	12.5	14.6	14.6	14.6
3	2	20.2	19.9	19.9	21.4	21.3	21.3
5	3	14.9	14.8	14.8	13.7	13.8	13.8
10	9	29.7	30.4	30.4	31.2	31.0	31.0

respectively) or including the two first H_2 rotational states ($j_2 = 0, 2$ and $j_2 = 1, 3$). As illustrated in Fig. 5, including only the first rotational state of *para*-H_2 leads to inaccuracies higher than 30%, in particular at low collision energies where the cross sections exhibit strong resonances. Considering collisions with *ortho*-H_2, the cross sections obtained with only the first rotational level ($j_2 = 1$) of H_2 or the two first levels ($j_2 = 1, 3$) lead to differences generally lower than 10% while a large increase by two orders of magnitude of the computational time is found. Hence, we have retained for the H_2 rotational basis set the first two rotational states ($j_2 = 0, 2$) of *para*-H_2 and only one rotational state ($j_2 = 1$) of *ortho*-H_2.

The collisional rate coefficients $k_{j_1,j_2 \to j_1',j_2}(T)$ were derived for temperatures up to 100 K by averaging the computed cross sections $\sigma_{j_1,j_2 \to j_1',j_2}(E_k)$ as:

$$k_{j_1,j_2 \to j_1',j_2}(T) = \left(\frac{8k_BT}{\pi\mu}\right)^{\frac{1}{2}} \left(\frac{1}{k_BT}\right)^2 \times \int_0^\infty E_k \, \sigma_{j_1,j_2 \to j_1',j_2}(E_k) \, e^{\frac{-E_k}{k_BT}} dE_k, \tag{2}$$

where E_k is the collision energy, $\mu = 1.86555$ au is the reduced mass of the complex, and k_B is the Boltzmann constant. In this paper, we only consider transitions where H_2 remains in its first rotational level ($j_2 = 0$), as rotational excitation of $H_2(j_2 = 2)$ has a very low probability at the considered range of energies.

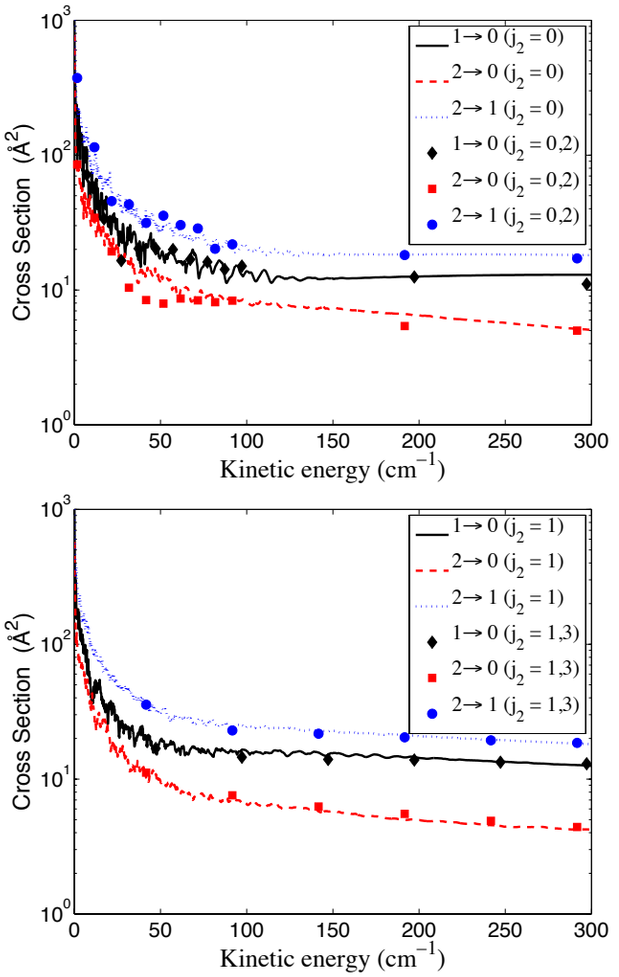

FIG. 5. Comparison of C_2H^- rotational de-excitation cross sections for selected rotational transitions $j_1 \rightarrow j_1'$, including only the first (lines) or the two first (symbols) rotational states in the H_2 basis.

IV. RESULTS

Figure 6 (upper panel) displays the energy variation of the cross sections for de-excitation of C_2H^- by collision with *para*- and *ortho*-H_2 for selected transitions. The cross sections present the same behavior for both H_2 species with a decrease with increasing energy, following a quasi-linear dependence as a function of the energy logarithm. This behavior, predicted by the Langevin theory, is typical of ion-molecule collisions.[35,50–54] The cross sections exhibit large resonances for kinetic energies up to 100 cm^{-1}. This is a consequence of the formation of bound and quasi-bound states within the deep well of the C_2H^-–H_2 complex before

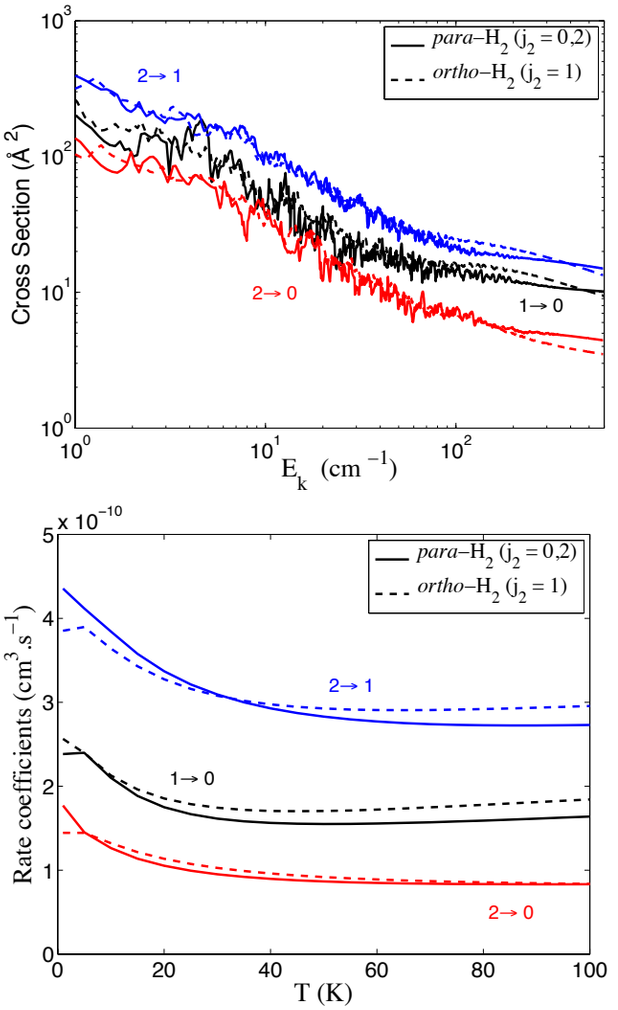

FIG. 6. Variation of the rotational cross sections and rate coefficients (in cm^3s^{-1}) for selected transitions of C_2H^- induced by collisions with *para*-$H_2(j_2 = 0, 2)$ (solid lines) and *ortho*-$H_2(j_2 = 1)$ (dashed lines).

it dissociates. At higher energies, resonances tend to wash out due to the contribution of high values of the total angular momentum J_{tot} with no more bound or quasi-bound states. Moreover, as was also found for other ionic systems in collision with *para*- and *ortho*-H_2, both projectiles lead to similar cross sections. Consequently, the corresponding rate coefficients (see Fig. 6, lower panel) have a very similar magnitude and show a relatively flat temperature dependence, in agreement with the Langevin theory. It is worth noting that, as found for the cross sections, the rate coefficients for collisions with *para*-H_2 obtained using an H_2 basis set with only the first H_2 level differ from those obtained with two H_2 levels,

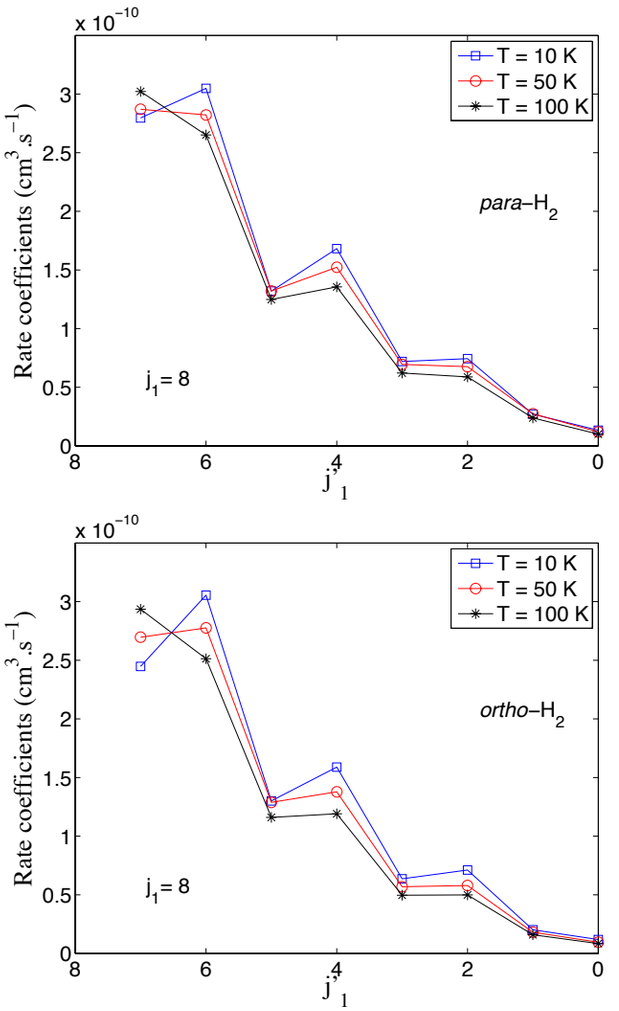

FIG. 7. Rotational de-excitation rate coefficients of C_2H^- in collision with *para*-H_2 and *ortho*-H_2 from C_2H^- (j_1=8) to C_2H^- (j_1').

with differences up to 20–30%.

In Fig. 7, we present de-excitation rate coefficients out of the $C_2H^-(j_1 = 8)$ level induced by *para*- and *ortho*-H_2 collisions and at temperatures of 10, 50 and 100 K. As can be seen in the figure, transitions with $\Delta j_1 = 1$ and 2 are dominant for both *para*- and *ortho*-H_2 projectiles, with rate coefficients close in magnitude and with a slight propensity for $\Delta j_1 = 2$ at low temperatures. For larger values of Δj_1, the rate coefficients decrease with increasing Δj_1, with a propensity for even Δj_1. Such propensity was also found by Toumi *et al.*[28] in their study of the rotational excitation of C_2H^- by collision with *para*-$H_2(j_2 = 0)$ using a 2D-PES. This averaged PES exhibits an almost near-homonuclear symmetry leading to

propensity rules in favor of even Δj_1. Figure 8 displays the rate coefficients obtained by Toumi *et al.*[28] as a function of those obtained in this work for all collisional transitions of C_2H^- by para $H_2(j_2 = 0)$ at 50 K.

Differences within 30% are observed between the two sets of rate coefficients. These differences are either due to the different levels of electronic structure theory used to generate the PESs, or to the use of an averaged 2D-PES neglecting the H_2 orientation. To differentiate the impact of these 2 possibilities, we have derived a 2D-PES (hereafter PES-2D-AV) from an average of our full 4D-PES using the same three H_2 orientations reported by Toumi *et al.*[28] Figure 9 presents a comparison of the rate coefficients from Toumi *et al.* as a function of those obtained using our averaged potential PES-2D-AV. The agreement between the two sets of data is good. This highlights that, for this system, the use of a 2D-PES obtained by an average over three H_2 orientations does not allow to obtain results with an accuracy better than 30%. Bop *et al.*[29] obtain a similar conclusion in the study of rotational excitation of NS^+ by *para*-H_2. This shows the need for using a PES describing all orientations of H_2 in cases where the PES exhibits large anisotropies at R-distances dominant for the nuclear dynamics. It is worth noting that this result is unusual as, for other ionic systems, a better agreement (20% or less) is found between full and dimensionality-reduced approaches.[52,54,55]

Finally, as previously found by Toumi *et al.*,[28] the present results show that collisional rate coefficients with *para*-H_2 differ by large factors, up to ten, from values obtained for collisions with He,[56] that cannot be used to reliably model the rate coefficients with H_2.

V. CONCLUSION

We have computed the first 4D PES for the C_2H^-–H_2 vdW system at the CCSD(T)-F12b level of theory, extrapolated to the complete basis set limit. The global minimum corresponds to a linear geometry with H_2 at the C-end of C_2H^- with a well-depth of 924.96 cm^{-1} and a distance between the two centers-of-mass of $R = 3.686$ Å. Close-coupling scattering calculations for collisional excitation by *para*- and *ortho*-H_2 were performed using this new high-level PES. State-to-state cross sections between the first 11 rotational levels of C_2H^- were computed for energies up to 1000 cm^{-1}, leading to rate coefficients for temperatures in the 1–100 K range. The results can be summarized as follows:

- The inelastic cross sections for collisions with *para*- and *ortho*-H_2 are very similar in

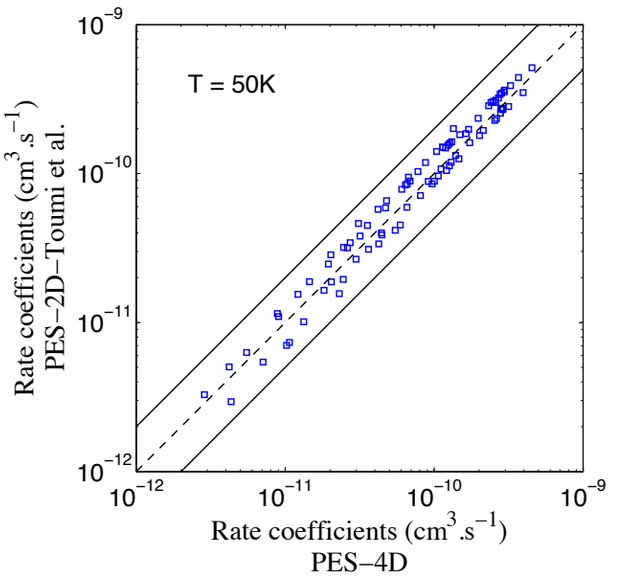

FIG. 8. Comparison between rate coefficients at 50 K obtained in the present work with the PES-4D and those of Toumi *et al.*[28] for collisional excitation with *para*-H_2 ($j_2 = 0$) of all the $j_1 \rightarrow j_1'$ C_2H^- transitions. The two black lines delimit the region where the sets of data differ by less than a factor of 2 and the dashed line corresponds to equal values of the data.

magnitude; except at low energies, where many resonances are present. A similar conclusion is found for the rate coefficients.

- Rate coefficients for transitions with Δj_1=1,2 are dominant for both species. For larger Δj_1 transitions, the rate coefficients decrease with a propensity for even Δj_1.

- Accurate calculation of cross sections and rate coefficients require the inclusion of $j_2 = 0$ and $j_2 = 2$ in the H_2 basis set for collision with *para*-H_2 and, while for collisions with *ortho*-H_2, the inclusion of $j_2 = 1$ is sufficient.

- The explicit description of the anisotropy of the PES with respect to the orientation of H_2 is required, as using an averaged 2D-PES led to deviations of 20–30% of the corresponding *para*-H_2 rate coefficients.

The data presented in this work could help in searching C_2H^- via non-LTE models which could indicate the most intense lines.

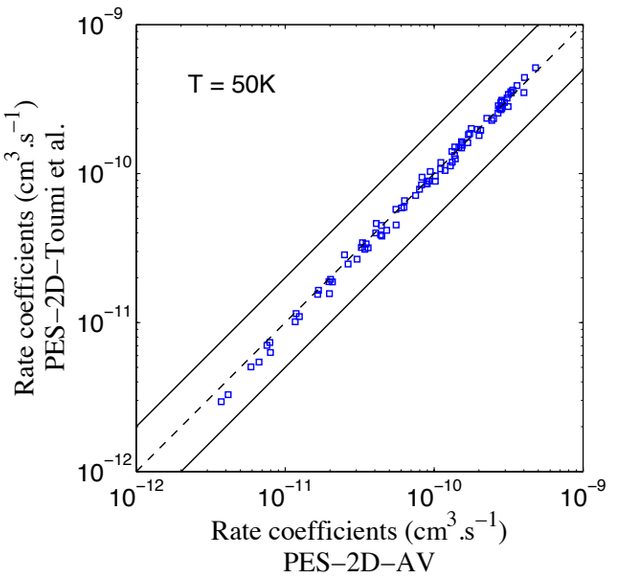

FIG. 9. Comparison between rate coefficients obtained at 50 K with the present averaged PES-2D-AV with those of Toumi *et al.*[28] for collisional excitation with *para*-H_2 ($j_2 = 0$) of all the $j_1 \rightarrow j_1'$ C_2H^- transitions. The two black lines delimit the region where the sets of data differ by less than a factor of 2 and the dashed line corresponds to equal values of the data.

SUPPLEMENTARY MATERIAL

A Fortran routine of the potential energy surface is available as the supplementary material.

ACKNOWLEDGMENTS

This work was supported by the CNRS programs "Physique et Chimie du Milieu Interstellaire (PCMI)" co-funded by the "Centre National d'Etudes Spatiales (CNES)" and "Programme National de Physique Stellaire (PNPS)". Part of the calculation was performed using HPC resources from GENCI-[CINES/IDRIS] (grant N°2010040883) and workstations at the "Centre Informatique" of Paris Observatory. This work was also granted access to the HPC resources of MesoPSL financed by the "Région Île de France" and the project Equip@Meso (reference ANR-10-EQPX-29-01) of the "programme Investissements d'Avenir" supervised by the "Agence Nationale pour la Recherche". R.D. and E.Q.-S. are supported by the U.S. Department of Energy (Award DE-SC0019740). Computing resources were supported by

the National Science Foundation under Grant No. OAC-1919789.

DATA AVAILABILITY

The data that support the findings of this study are available from the corresponding author upon request.

REFERENCES

[1]A. Dalgarno and R. A. McCray, ApJ **181**, 95 (1973).

[2]H. Herbst, Nature **289**, 656 (1981).

[3]M. C. McCarthy, C. A. Gottlieb, H. Gupta, and P. Thaddeus, ApJ **652**, L141 (2006).

[4]K. Kawaguchi, Y. Kasai, S.-I. Ishikawa, and N. Kaifu, PASJ **47**, 853 (1995).

[5]J. Cernicharo, M. Guélin, M. Agündez, K. Kawaguchi, M. McCarthy, and P. Thaddeus, A&A **467**, L37 (2007).

[6]M. Agúndez, J. Cernicharo, M. Guélin, M. Gerin, M. C. McCarthy, and P. Thaddeus, A&A **478**, L19 (2008).

[7]N. Sakai, T. Sakai, and S. Yamamoto, ApJ **673**, L71 (2008).

[8]A. J. Remijan, J. M. Hollis, F. J. Lovas, M. A. Cordiner, T. J. Millar, A. J. Markwick-Kemper, and P. R. Jewell, ApJ **664**, L47 (2007).

[9]K. Kawaguchi, R. Fujimori, S. Aimi, S. Takano, E. Y. Okabayashi, H. Gupta, S. Brünken, C. A. Gottlieb, M. C. McCarthy, and P. Thaddeus, PASJ **59**, L47 (2007).

[10]S. Brünken, H. Gupta, C. A. Gottlieb, M. C. McCarthy, and P. Thaddeus, ApJ **664**, L43 (2007).

[11]M. Agúndez, J. Cernicharo, M. Guélin, C. Kahane, E. Roueff, J. Kłos, F. J. Aoiz, F. Lique, N. Marcelino, J. R. Goicoechea, M. González García, C. A. Gottlieb, M. C. McCarthy, and P. Thaddeus, A&A **517**, L2 (2010).

[12]P. Thaddeus, C. A. Gottlieb, H. Gupta, S. Brünken, M. C. McCarthy, M. Agúndez, M. Guélin, and J. Cernicharo, ApJ **677**, 1132-1139 (2008).

[13]J. Cernicharo, M. Guélin, M. Agúndez, M. C. McCarthy, and P. Thaddeus, ApJ **688**, L83 (2008).

[14]J. Cernicharo, J. Pardo, C. Cabezas, M. Agundez, B. Tercero, N. Marcelino, R. Fuentetaja, M. Guelin, and P. de Vicente, A&A **670**, L19 (2023).

[15]P. J. Sarre, J. Chim. Phys. **77**, 769 (1980).

[16]E. Herbst and Y. Osamura, ApJ **679**, 1670 (2008).

[17]C. Walsh, N. Harada, E. Herbst, and T. J. Millar, ApJ **700**, 752 (2009).

[18]B. Eichelberger, T. P. Snow, C. Barckholtz, and V. M. Bierbaum, ApJ **667**, 1283 (2007).

[19]T. J. Millar, C. Walsh, and T. A. Field, Chem. Rev. **117**, 1765 (2017).

[20]T. Amano, J. Chem. Phys. **129**, 244305 (2008).

[21]K. D. Tucker, M. L. Kutner, and P. Thaddeus, ApJ **193**, L115 (1974).

[22]C. Barckholtz, T. P. Snow, and V. M. Bierbaum, ApJ **547**, L171 (2001).

[23]B. Eichelberger, T. P. Snow, C. Barckholtz, and V. M. Bierbaum, ApJ **667**, 1283 (2007).

[24]F. A. Gianturco, L. González-Sánchez, B. P. Mant, and R. Wester, J. Chem. Phys. **151**, 144304 (2019).

[25]J. Franz, B. P. Mant, L. González-Sánchez, R. Wester, and F. A. Gianturco, J. Chem. Phys. **152**, 234303 (2020).

[26]B. Mant, J. Franz, R. Wester, and F. A. Gianturco, Mol. Phys. **119**, e1938267 (2021).

[27]L. González-Sánchez, E. Yurtsever, B. P. Mant, R. Wester, and F. A. Gianturco, Physical Chemistry Chemical Physics (Incorporating Faraday Transactions) **23**, 7703 (2021).

[28]I. Toumi, O. Yazidi, and F. Najar, RSC Adv. **11**, 13579 (2021).

[29]C. T. Bop, Y. Kalugina, and F. Lique, J. Chem. Phys. **156**, 204311 (2022).

[30]G. Knizia, T. B. Adler, and H.-J. Werner, J. Chem. Phys. **130**, 054104 (2009).

[31]K. A. Peterson, T. B. Adler, and H.-J. Werner, J. Chem. Phys. **128**, 084102 (2008).

[32]D. Feller, K. A. Peterson, and T. D. Crawford, J. Chem. Phys. **124**, 054107 (2006).

[33]H.-J. Werner, P. J. Knowles, G. Knizia, F. R. Manby, and M. Schütz, Wiley Interdisciplinary Reviews: Computational Molecular Science **2**, 242 (2012).

[34]E. Castro-Juárez, X.-G. Wang, T. Carrington Jr, E. Quintas-Sánchez, and R. Dawes, J. Chem. Phys. **151**, 084307 (2019).

[35]B. Desrousseaux, E. Quintas-Sánchez, R. Dawes, and F. Lique, The Journal of Physical Chemistry A **123**, 9637 (2019).

[36]C. T. Bop, F. A. Batista-Romero, A. Faure, E. Quintas-Sánchez, R. Dawes, and F. Lique, ACS Earth and Space Chemistry **3**, 1151 (2019).

[37]E. Quintas-Sánchez, R. Dawes, X.-G. Wang, and T. Carrington, Physical Chemistry Chemical Physics **22**, 22674 (2020).

[38]B. Desrousseaux, E. Quintas-Sánchez, R. Dawes, S. Marinakis, and F. Lique, J. Chem. Phys. **154**, 034304 (2021).

[39]M. Gancewski, H. Jóźwiak, E. Quintas-Sánchez, R. Dawes, F. Thibault, and P. Wcisło, J. Chem. Phys. **155**, 124307 (2021).

[40]C. Balança, E. Quintas-Sánchez, R. Dawes, F. Dumouchel, F. Lique, and N. Feautrier, MNRAS **508**, 1148 (2021).

[41]E. Quintas-Sánchez, R. Dawes, and O. Denis-Alpizar, Mol. Phys. **119**, e1980234 (2021).

[42]E. Quintas-Sánchez and R. Dawes, J. Chem. Inf. Model. **59**, 262 (2019).

[43]R. Dawes and E. Quintas-Sánchez, in *Reviews in Computational Chemistry vol. 31* (Wiley, 2018) Chap. 5, pp. 199–264.

[44]M. Majumder, S. A. Ndengué, and R. Dawes, Mol. Phys. **114**, 1 (2016).

[45]R. Dawes, X.-G. Wang, A. W. Jasper, and T. Carrington Jr, J. Chem. Phys. **133**, 134304 (2010).

[46]I. M. Sobol, USSR Computational Mathematics and Mathematical Physics **16**, 236 (1976).

[47]J. M. Hutson and S. Green, "MOLSCAT computer code, version 14 (1994), distributed by collaborative computational project no. 6 of the engineering and physical sciences research council (uk)," (1994).

[48]M. H. Alexander and D. E. Manolopoulos, J. Chem. Phys. **86**, 2044 (1987).

[49]S. Green, J. Chem. Phys. **62**, 2271 (1975).

[50]J. Kłos and F. Lique, MNRAS **418**, 271 (2011).

[51]H. Massó and L. Wiesenfeld, J. Chem. Phys. **141**, 184301 (2014).

[52]O. Denis-Alpizar, T. Stoecklin, A. Dutrey, and S. Guilloteau, MNRAS **497**, 4276 (2020).

[53]K. M. Walker, F. Lique, F. Dumouchel, and R. Dawes, MNRAS **466**, 831 (2017).

[54]C. Balança, Y. Scribano, J. Loreau, F. Lique, and N. Feautrier, MNRAS **495**, 2524 (2020).

[55]A. Spielfiedel, M. L. Senent, Y. Kalugina, Y. Scribano, C. Balança, F. Lique, and N. Feautrier, J. Chem. Phys. **143**, 024301 (2015).

[56]F. Dumouchel, A. Spielfiedel, M. L. Senent, and N. Feautrier, Chem. Phys. Lett. **533**, 6 (2012).

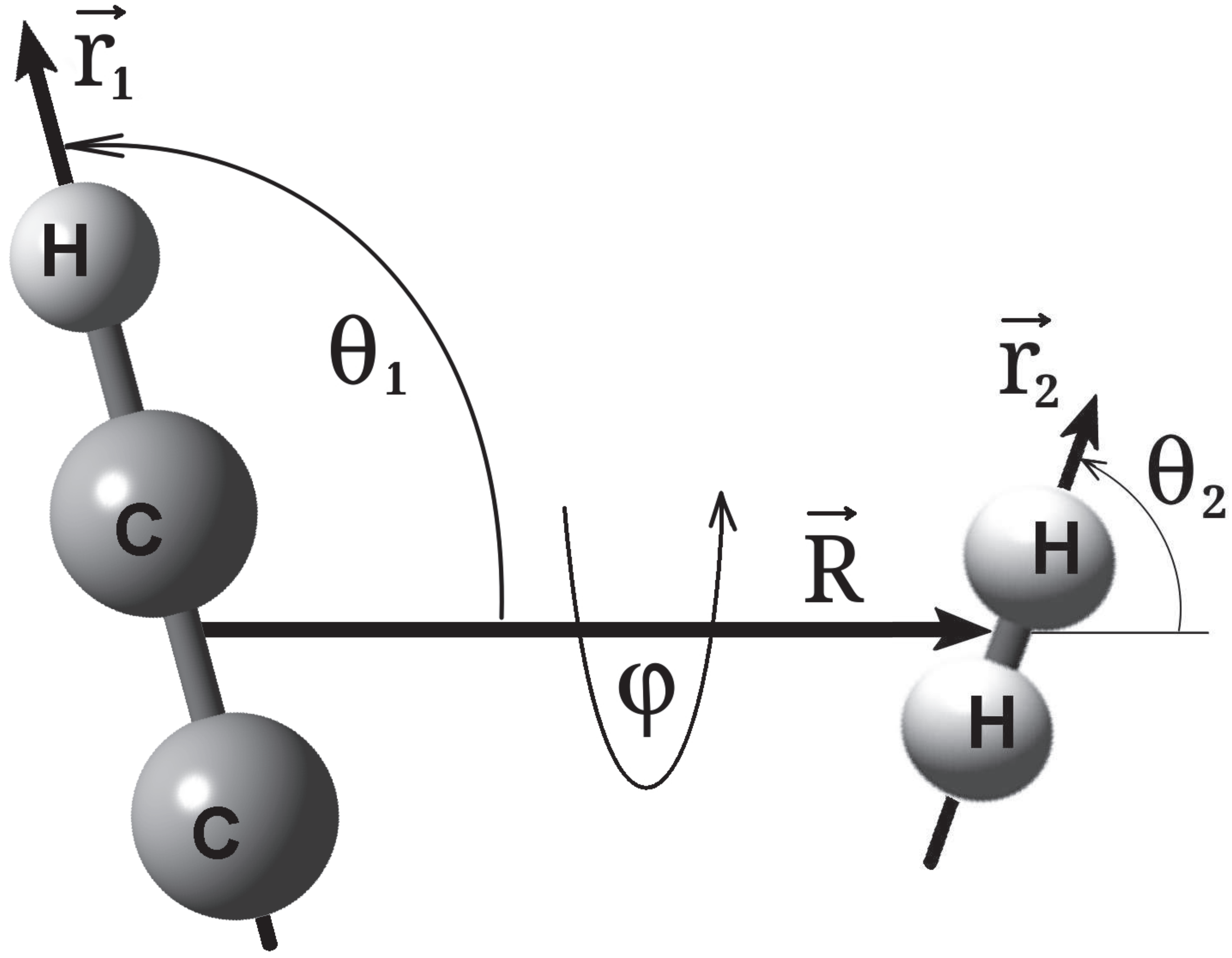
$\vec{r}_1$
H
θ_1
C
C
$\vec{r}_2$
θ_2
$\vec{R}$
H
H
φ

$\theta_1 = 180°;\ \varphi = 0°$

$\theta_1 = 90°;\ \varphi = 0°$

$R = 25.0$ Å

$R = 15.0$ Å

$R = 10.0$ Å

$R = 5.0$ Å

Potential (cm^{-1})

θ_2 (degrees)

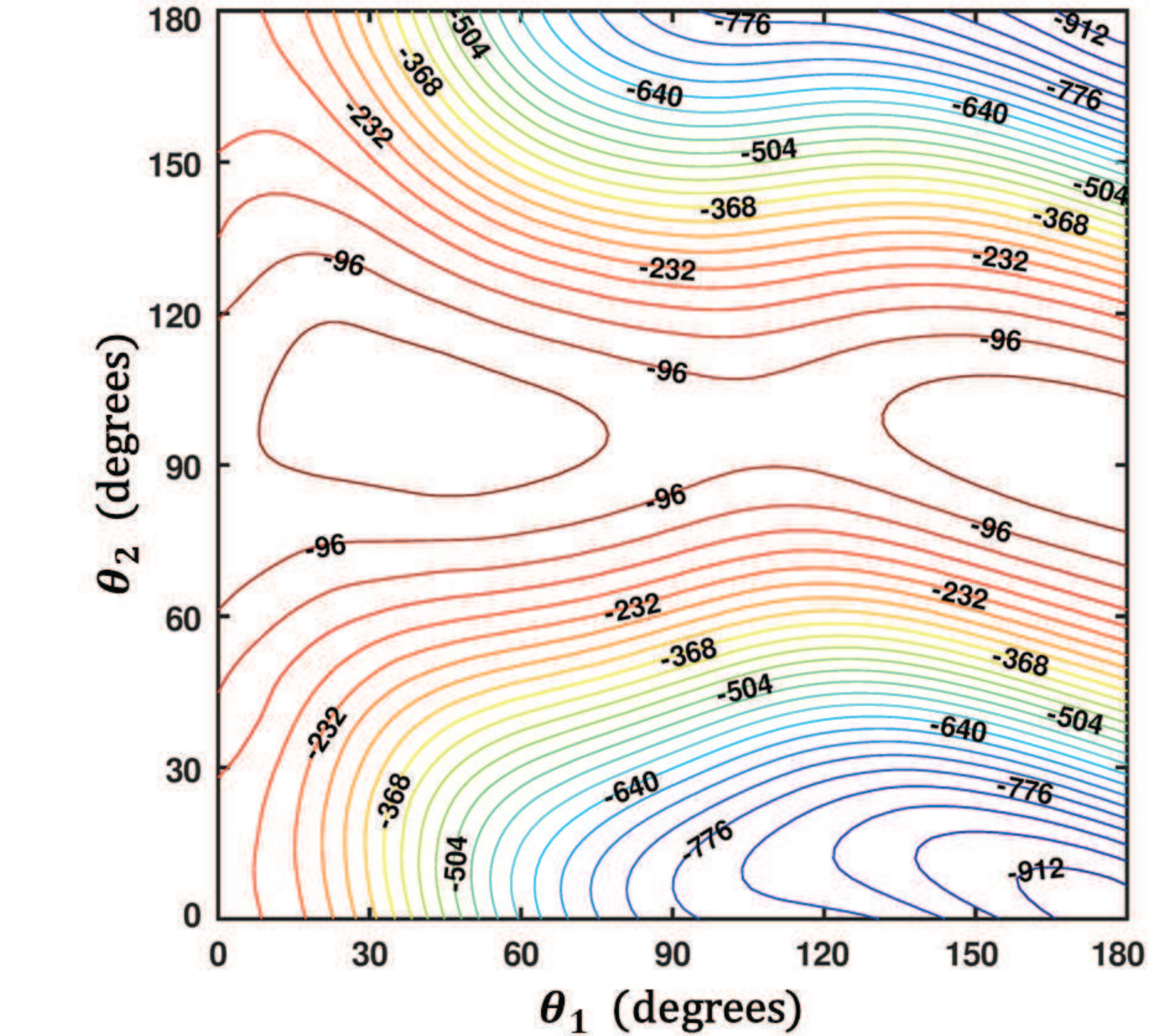
180
150
120
90
60
30
0
θ_2 (degrees)
0
30
60
90
120
150
180
θ_1 (degrees)
-96
-232
-368
-504
-640
-776
-912

400
200
0
-200
-400
-600
-800
-1000
$V\,(\mathrm{cm}^{-1})$
3
4
5
6
7
8
R (Å)
$\theta_1 = 0°; \theta_2 = 0°; \varphi = 0°$
$\theta_1 = 180°; \theta_2 = 0°; \varphi = 0°$
$\theta_1 = 90°; \theta_2 = 90°; \varphi = 0°$
$\theta_1 = 0°; \theta_2 = 90°; \varphi = 0°$
$\theta_1 = 180°; \theta_2 = 90°; \varphi = 0°$

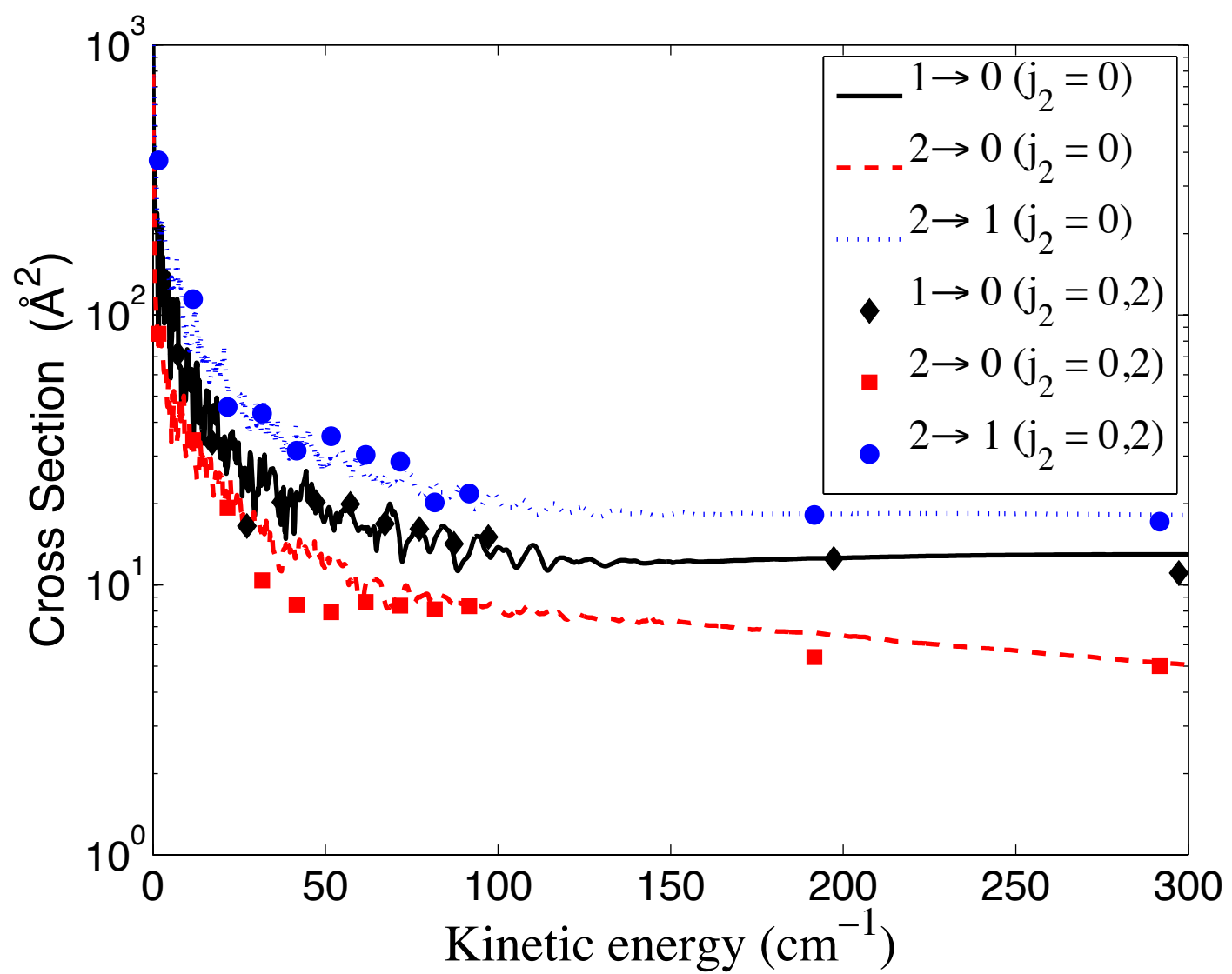
Cross Section (Å^2)
10^3
10^2
10^1
10^0
0
50
100
150
200
250
300
Kinetic energy (cm^{-1})
1→ 0 (j_2 = 0)
2→ 0 (j_2 = 0)
2→ 1 (j_2 = 0)
1→ 0 (j_2 = 0,2)
2→ 0 (j_2 = 0,2)
2→ 1 (j_2 = 0,2)

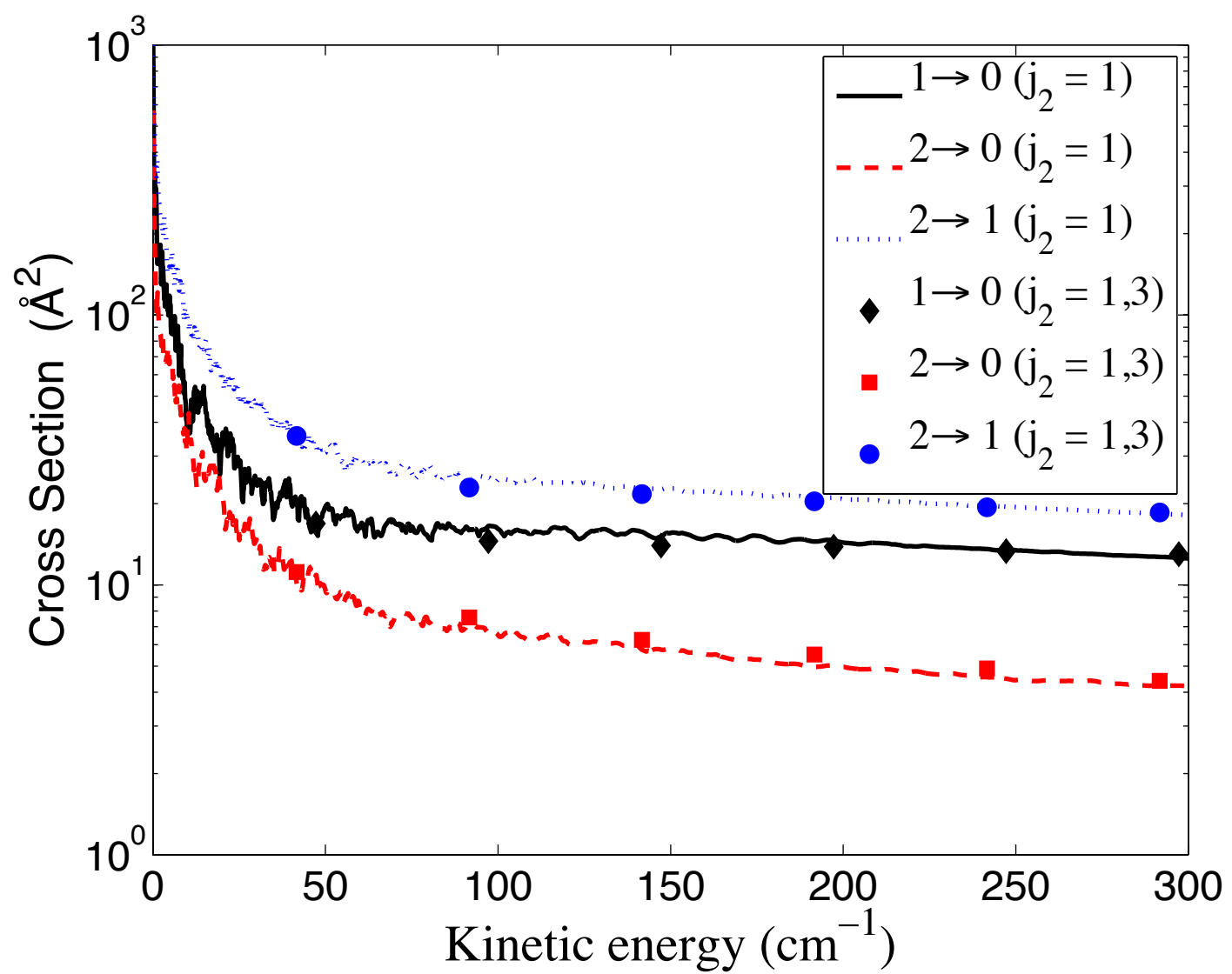
Cross Section (Å^2)
10^3
10^2
10^1
10^0
0
50
100
150
200
250
300
Kinetic energy (cm^{-1})
1→ 0 (j_2 = 1)
2→ 0 (j_2 = 1)
2→ 1 (j_2 = 1)
1→ 0 (j_2 = 1,3)
2→ 0 (j_2 = 1,3)
2→ 1 (j_2 = 1,3)

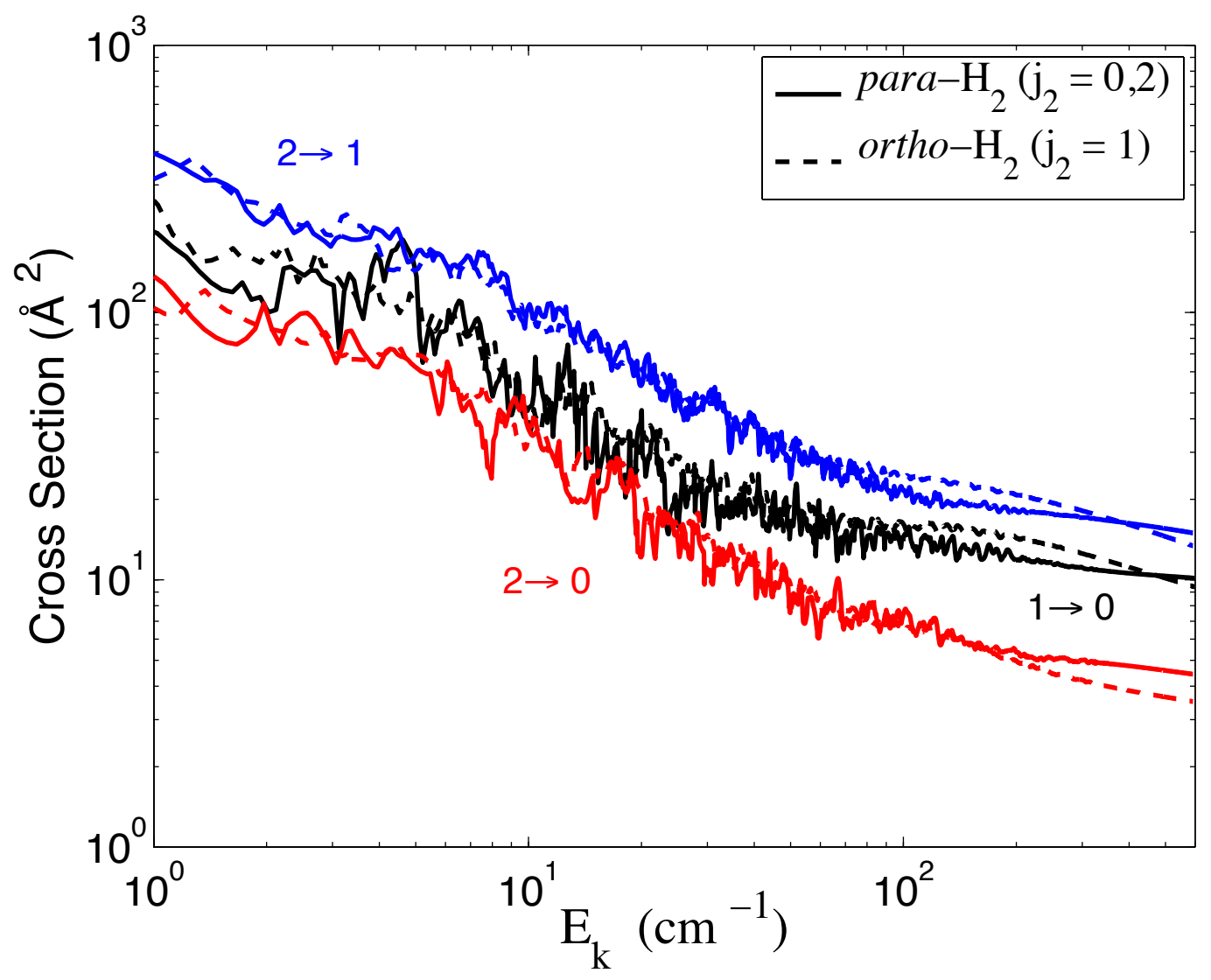
para–H2 (j2 = 0,2)
ortho–H2 (j2 = 1)
2→ 1
2→ 0
1→ 0
Cross Section (Å 2)
Ek (cm −1)
10^3
10^2
10^1
10^0
10^0
10^1
10^2

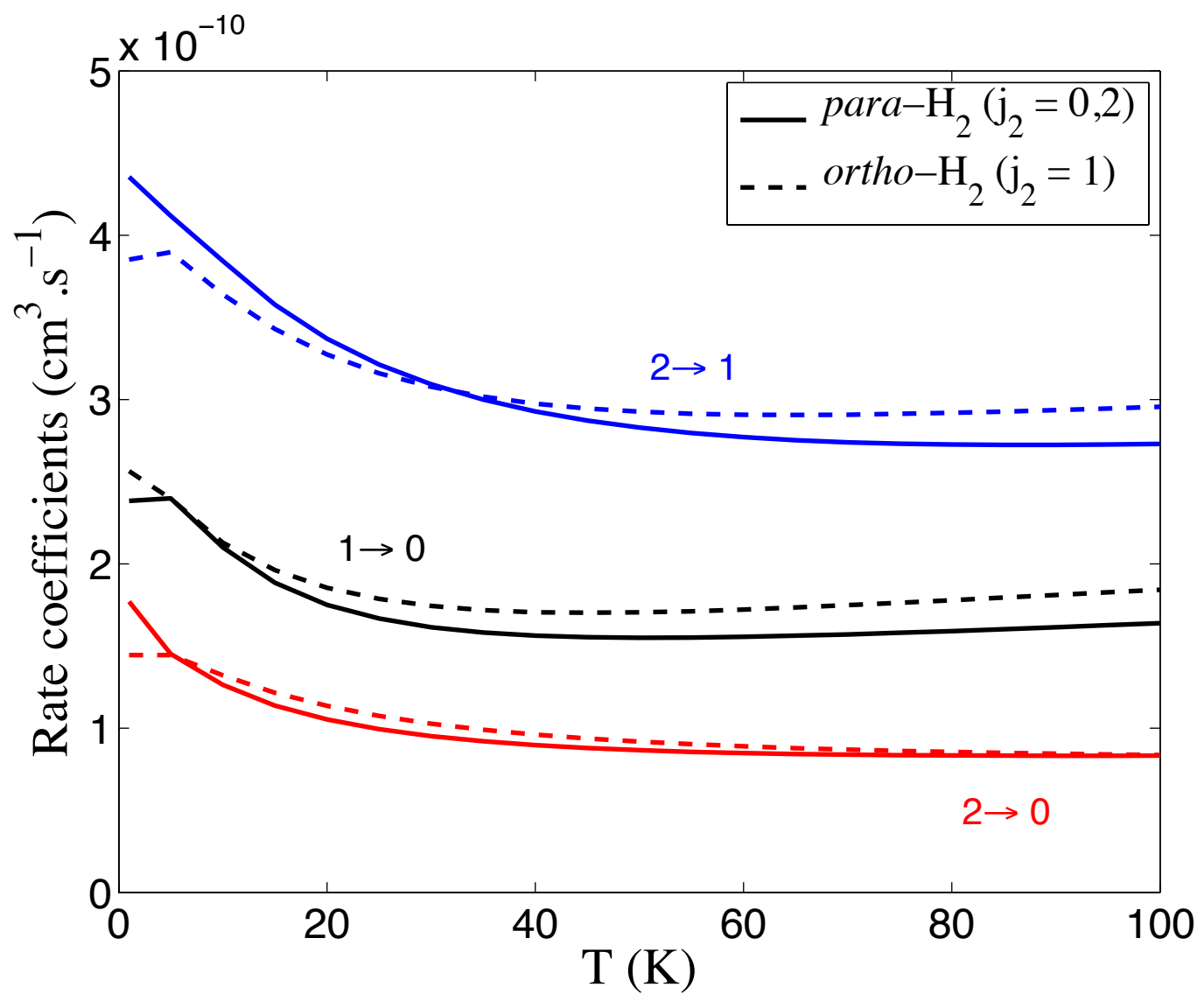
x 10^-10
5
4
3
2
1
0
Rate coefficients (cm^3 .s^-1)
0
20
40
60
80
100
T (K)
para–H2 (j2 = 0,2)
ortho–H2 (j2 = 1)
2→ 1
1→ 0
2→ 0

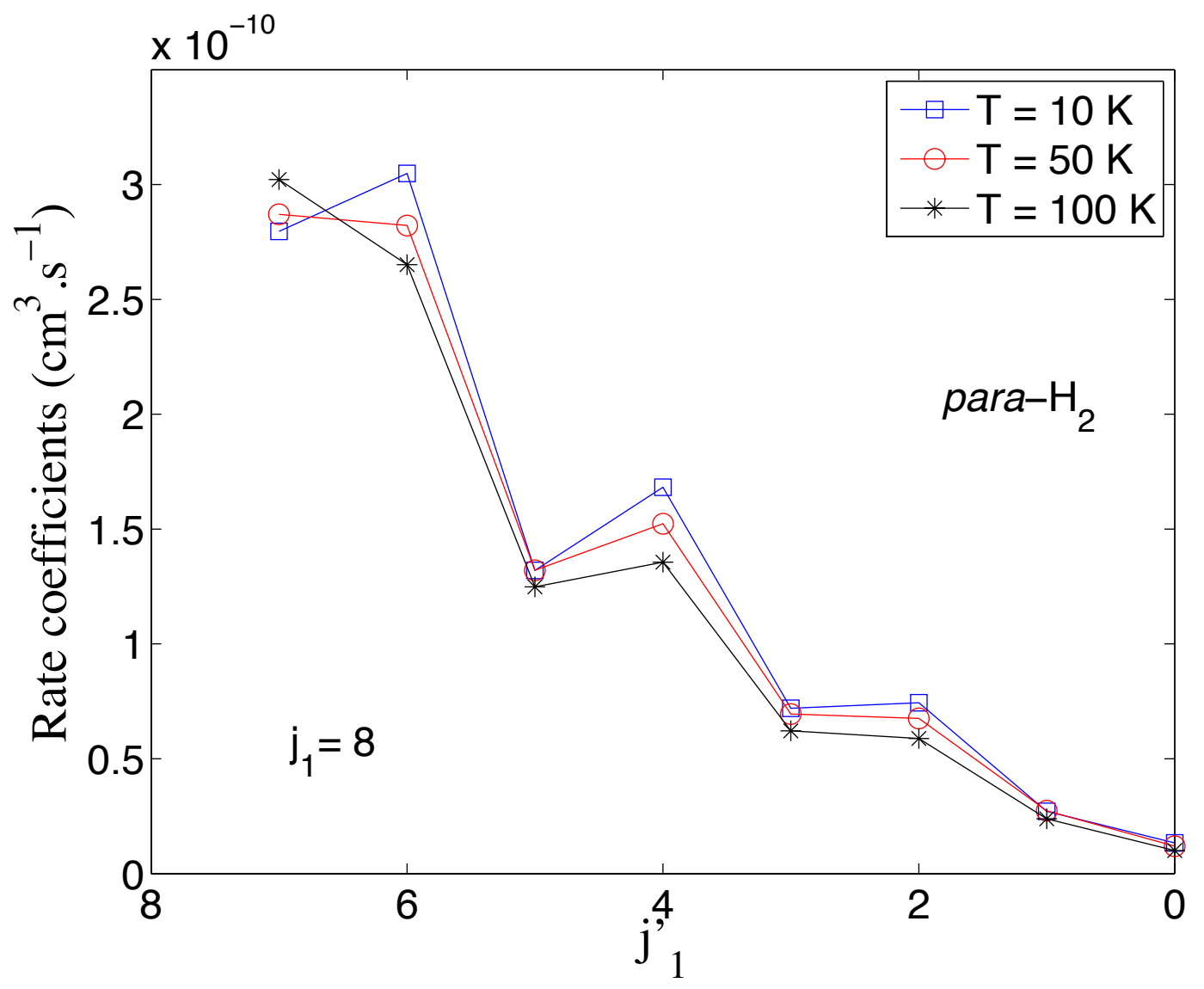
x 10^-10
Rate coefficients (cm^3.s^-1)
T = 10 K
T = 50 K
T = 100 K
para–H2
j1 = 8
j'1
0
0.5
1
1.5
2
2.5
3
8
6
4
2
0

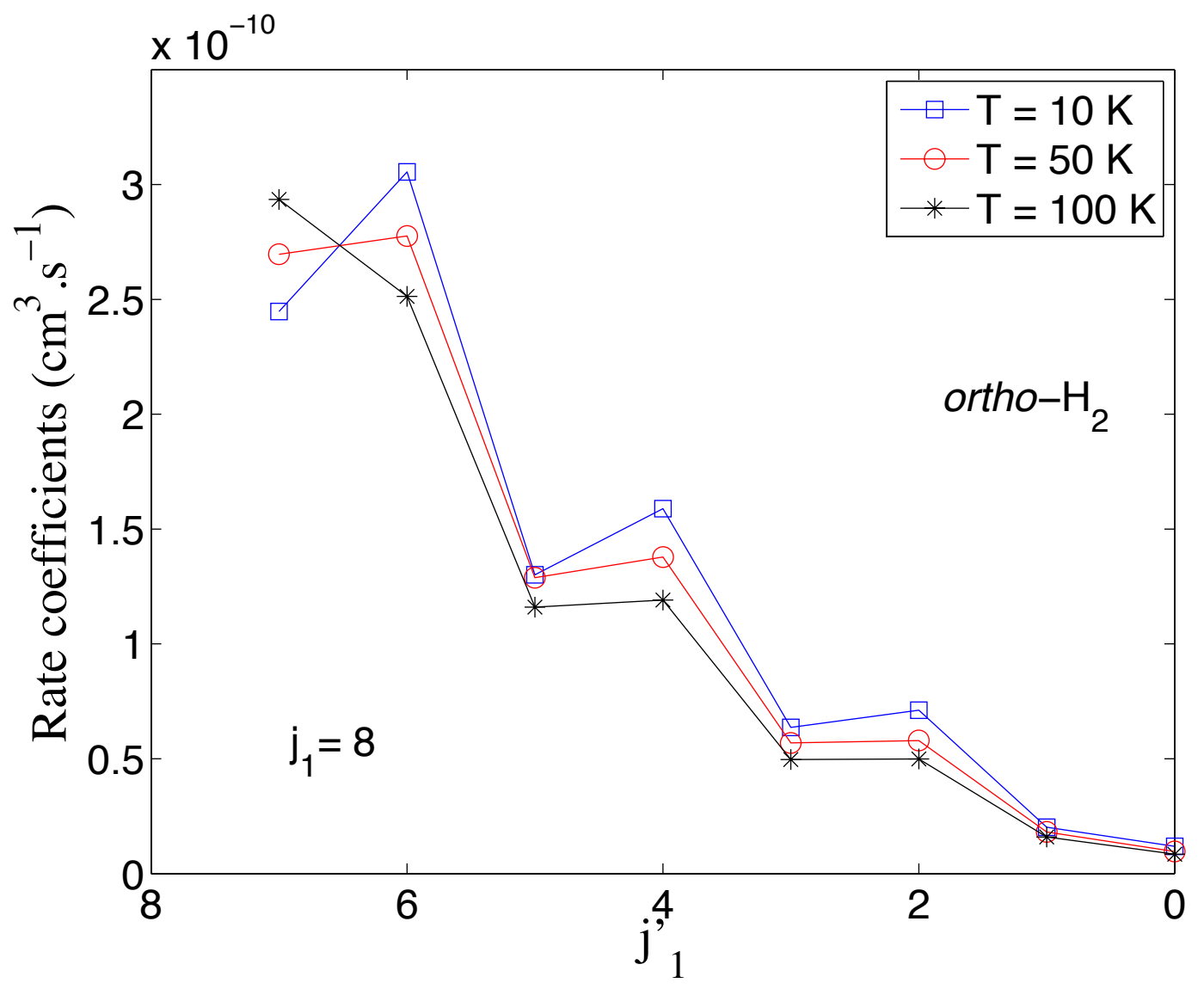
x 10^-10
Rate coefficients (cm^3.s^-1)
T = 10 K
T = 50 K
T = 100 K
ortho–H2
j1 = 8
j'1
0
0.5
1
1.5
2
2.5
3
8
6
4
2
0

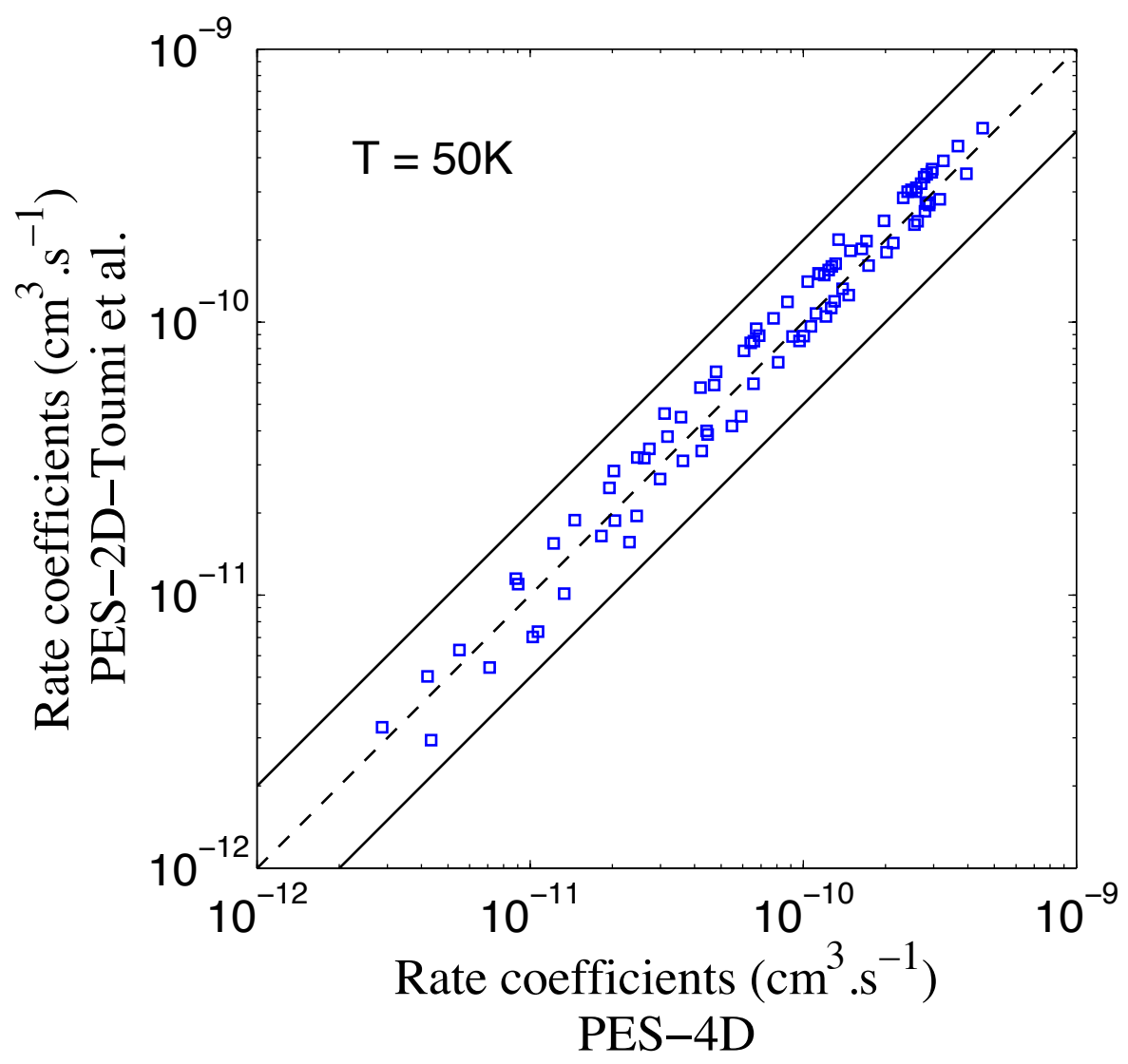
T = 50K
10^{-9}
10^{-10}
10^{-11}
10^{-12}
10^{-12}
10^{-11}
10^{-10}
10^{-9}
Rate coefficients ($cm^3.s^{-1}$)
PES−2D−Toumi et al.
Rate coefficients ($cm^3.s^{-1}$)
PES−4D

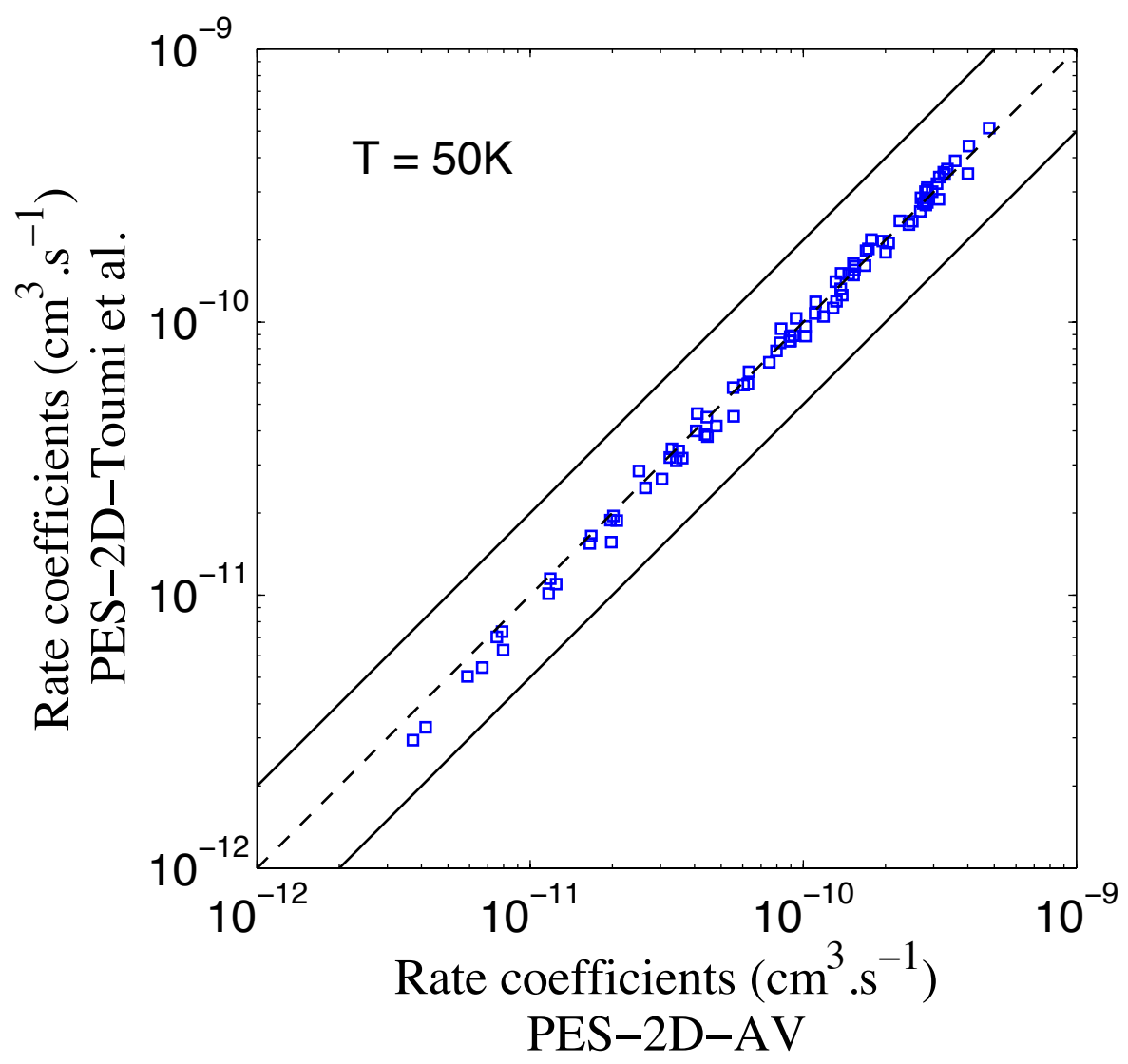
T = 50K
10^{-9}
10^{-10}
10^{-11}
10^{-12}
10^{-12}
10^{-11}
10^{-10}
10^{-9}
Rate coefficients ($cm^3.s^{-1}$)
PES−2D−Toumi et al.
Rate coefficients ($cm^3.s^{-1}$)
PES−2D−AV